

CHAPTER IV

RESULTS AND DISCUSSION

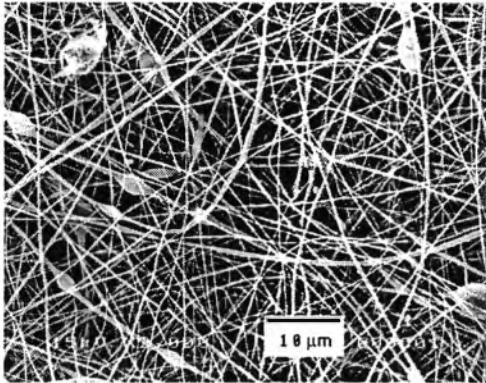
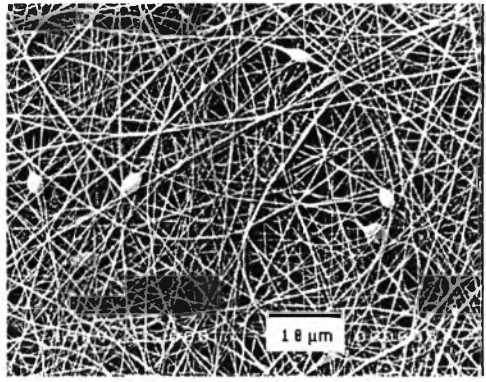
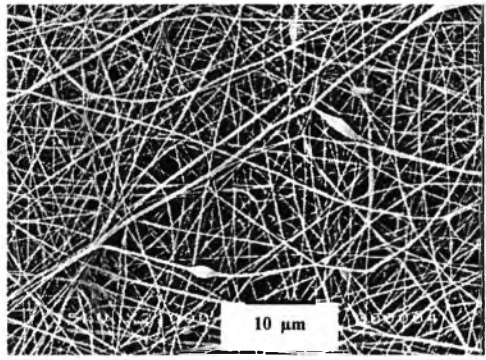
4.1 Morphology and microstructure of electrospun silk fibroin fibers

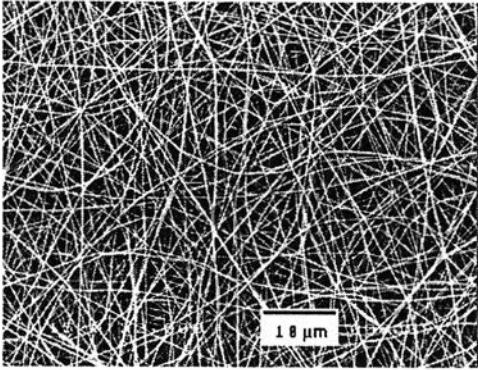
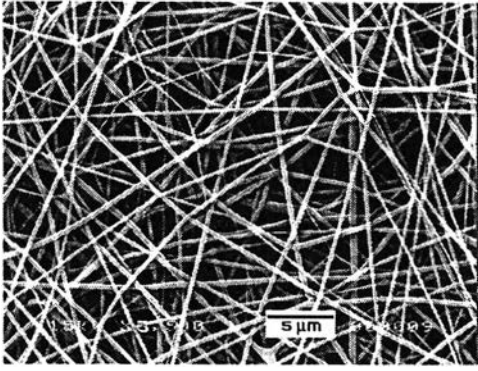
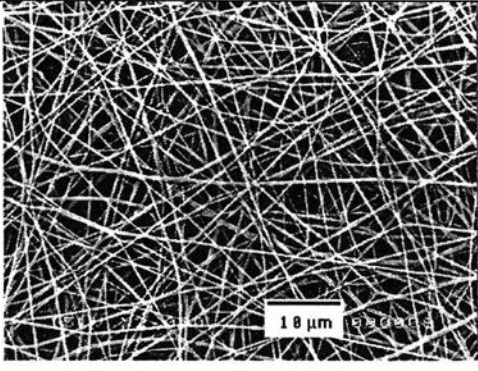
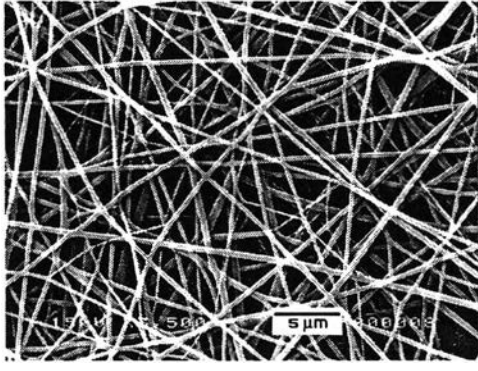
In order to study the effect of silk fibroin concentration in formic acid on the morphology of electrospun silk fibroin fibers, the concentration of silk fibroin solutions was varied from 42 to 52 % w/v, while other parameters were kept constant (needle gauge = 20, collection distance = 15 cm, and applied voltage = 25 kV). The selected SEM micrographs of the electrospun silk fibroin fibers obtained under different concentrations are shown in Table 4.1.

At the concentration 42 % w/v, no fibers were formed, due to the low viscosity of the solution. In this condition, the surface tension of polymer solution was the dominant factor controlling the morphology that resulted in the formation of as-sprayed droplets [11]. At a slightly greater concentration of the solution (i.e., 44% w/v), beaded fibers were formed, with the average diameter of the fiber segment between beads being about 250 nm. Beaded fibers were still observed when the concentration of the silk fibroin solution was lower than or equal to 48% w/v [27]. Only when the concentration of the solutions was greater than or equal to 50% w/v, electrospun fibers without the presence of beads were obtained. Clearly, the average diameter of the obtained fibers was an increase function of the concentration. Specifically, it increased from about 250 nm at the silk fibroin concentration of 44% w/v to about 329 nm at the silk fibroin concentration of 52% w/v.

Based on the results obtained, the minimum silk fibroin concentration that resulted in the formation of smooth electrospun silk fibroin fibers with the smallest average diameter was 50% w/v. Based on this observation, 50% w/v of the silk fibroin solution was electrospun into fibrous mats for further investigate the effect of the applied voltage on morphology of the electrospun silk fibroin fibers.

Table 4.1. SEM micrographs and average fiber diameter of electrospun silk fibroin fibers from silk fibroin solution with the concentrations ranging from 42 to 52% w/v.

Concentration % w/v	SEM micrographs	Average diameter (nm)
42	No fiber formation	-
44	 <p data-bbox="582 978 974 1017">(X 2000) Scale bar = 10 μm</p>	250 ± 74
46	 <p data-bbox="582 1461 974 1501">(X 2000) Scale bar = 10 μm</p>	264 ± 82
48	 <p data-bbox="582 1921 974 1961">(X 2000) Scale bar = 10 μm</p>	272 ± 92

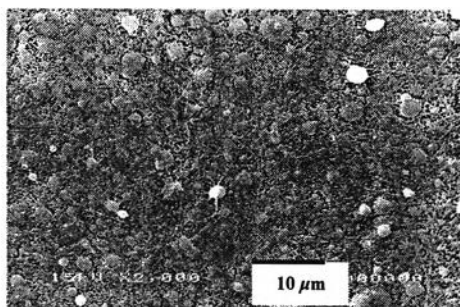
50	 <p>(X 2000) Scale bar = 10 μm</p>  <p>(X 3500) Scale bar = 5 μm</p>	329 ± 85
52	 <p>(X 2000) Scale bar = 10 μm</p>  <p>(X 3500) Scale bar = 5 μm</p>	417 ± 72

In electrospinning, the morphology of electrospun silk fibroin fibers was varied with the applied voltages from a high voltage power supply and the concentrations of silk fibroin in formic acid.

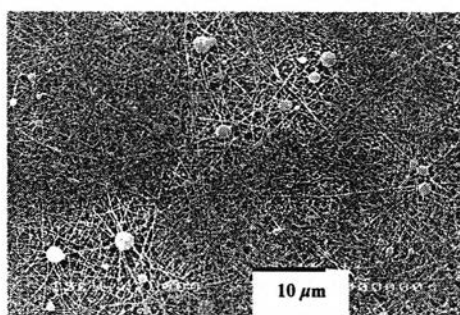
In order to study the effect of applied voltage on morphology of the electrospun silk fibroin fibers, the applied voltage was varied (15 – 30 kV), while all other parameters were kept constant (needle gauge = 20, collection distance = 15 cm, and concentration of the silk fibroin solution = 50 % w/v). Selected SEM micrographs of the electrospun silk fibroin fibers obtained under different applied voltages are shown in Fig. 4.1. Initially, the silk fibroin solution is held by its surface tension in the form of a droplet at a tip of the needle. As the applied voltage increased, charges were induced on the fluid surface, creating forces directly opposite to the surface tension, causing the distortion of the shape of the droplet [10,12].

At the low applied voltages of 15 and 20 kV (Fig.4.1a, b) electrospinning of the solution generated beads and beaded fibers, respectively, due to the relatively low Coulombic repulsion force that is lower than the surface tension of silk fibroin solution. At 25 kV (Fig. 4.1c), the Coulombic repulsion force was high enough to counter the surface tension, resulting in the formation of continuous fibers without the presence of beads with average diameter 333 ± 44 nm. At even higher applied voltage of 30 kV (Fig. 4.1d), reestablishment of the beaded fibers was observed, due to inconsistency in the flow of the material. In other words, at such a high applied voltage, the force exerting on the jet due to the electric field was high, causing the jet to neck down or even broke off. Both the necking and the breaking off of the jet could result in the formation of beaded fibers [11].

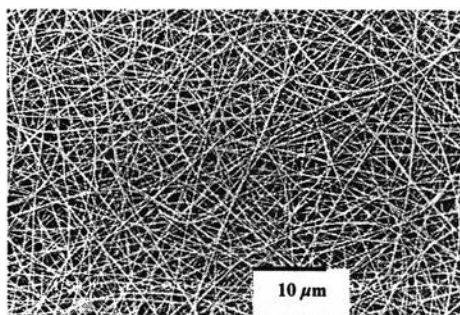
Based on these results, the optimal applied voltage among those investigated was 25 kV.



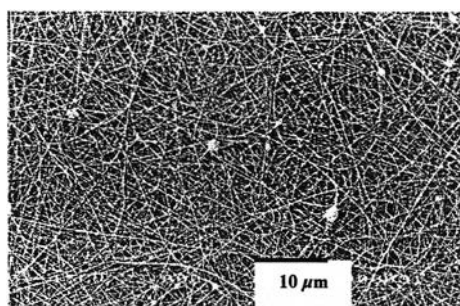
(a) 15 kV ; No fibers formation



(b) 20 kV ; Average diameter = 234 ± 54 nm



(c) 25 kV ; Average diameter = 333 ± 44 nm



(d) 30 kV ; Average diameter = 244 ± 65 nm

Fig. 4.1 SEM micrographs of electrospun silk fibroin fibers obtained with the different applied voltages ranging from 15 to 30 kV.

4.2 Thermogravimetric analysis of electrospun silk fibroin fibers

The TGA thermogram of electrospun silk fibroin fibers is shown in Fig. 4.2. The electrospun silk fibroin fibers was tested under nitrogen atmosphere at a heating rate of 10 °C/min, exhibiting an initial weight loss beginning at above 50 °C to about 100 °C due to the evaporation of moisture content in the electrospun silk fibroin fibers. As the temperature were continuously increased, the electrospun silk fibroin fibers remained stable until about 270 °C, when the TGA curve started to decline to indicate the beginning of the thermal decomposition. Afterward, a greater weight loss was occurred to about 370 °C. This is associated with the breakdown of side groups belonging to amino acid residues as well as the cleavage of the peptide bonds [18, 28].

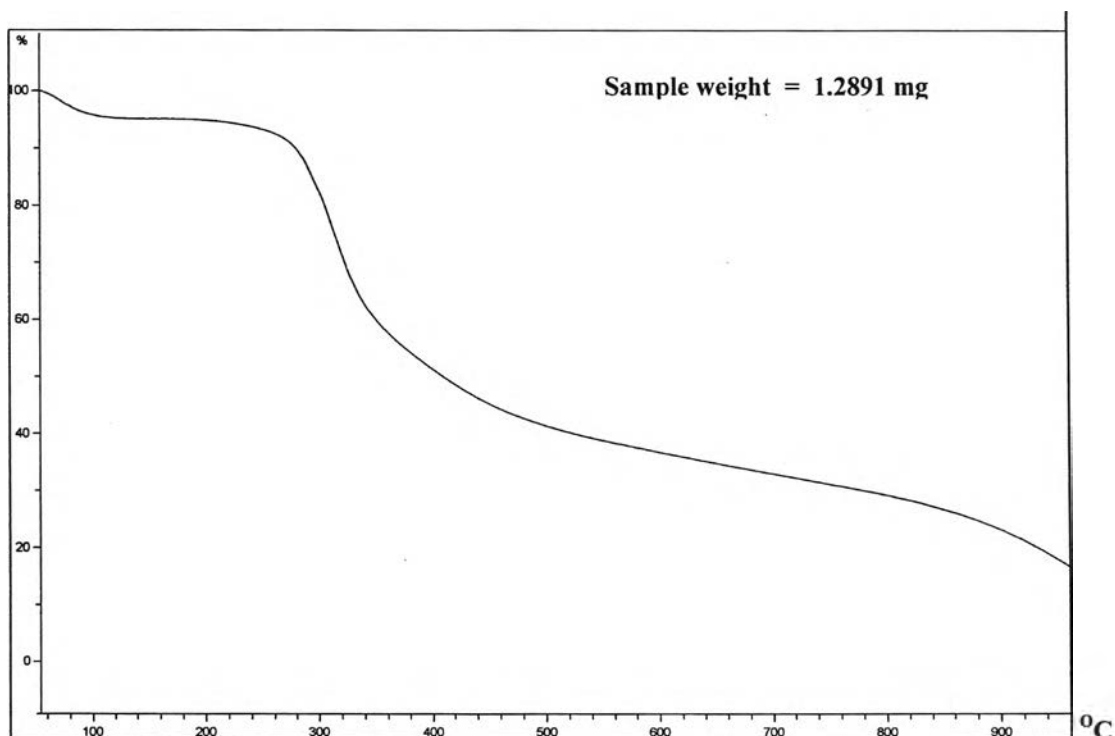


Fig. 4.2 Thermogravimetric analytical curve of electrospun silk fibroin fibers

4.3 Infrared analysis of electrospun silk fibroin fibers

The chemical characteristics of the electrospun silk fibroin fibers was studied by ATR-FTIR spectroscopy. Fig. 4.3 shows the IR spectra of electrospun silk fibroin fibers in the range 4000-400 cm^{-1} . The spectrum was characterized by the absorption bands at 1623 cm^{-1} (amide I), 1528 cm^{-1} (amide II), 1247 cm^{-1} (amide III) and 680 cm^{-1} (amide V) assigned to the β -sheet conformation [28,29]. The peaks at 1623, 1441, and 1156 was corresponding to the stretching vibration of C=O (carboxyl amide I group), CH_3 , and $-\text{C}-\text{O}-\text{C}-$ bond. It should be noted that the β -sheet conformation was introduced after the electrospun silk fibroin fibers were treated with the methanol solution.

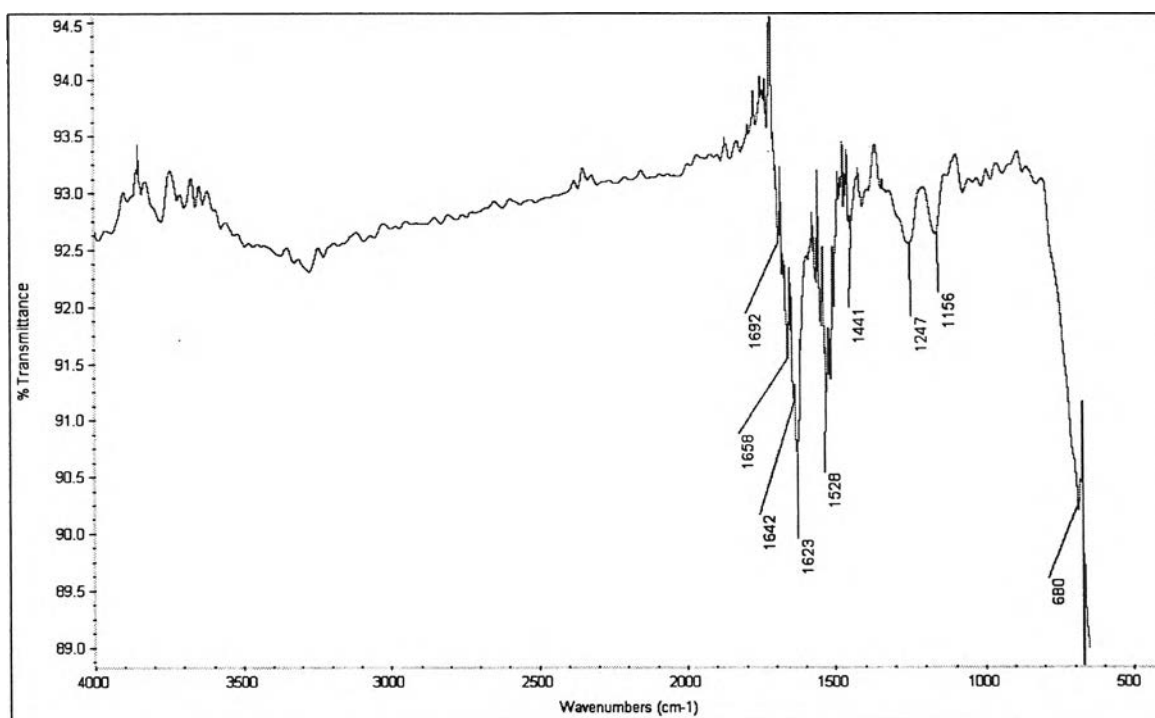


Fig. 4.3 ATR-FTIR spectrum of electrospun silk fibroin fibers

4.4 Cytotoxicity tests

Cytotoxicity test was used to investigate the biocompatibility of the silk fibroin scaffolds, both fibrous mats and films. Schwann cells were used in order to evaluate the potential for using silk fibroin for nerve regeneration. Recently, Sundback et al. [26] examined the possibility for the use of poly(glycerol sebacate) as a nerve guide material. They carried out the cytotoxicity evaluation of the material using Schwann cells as reference. They reported that poly(glycerol sebacate) is an excellent candidate material for neural reconstruction applications, due to the non-toxicity of Schwann cells [26].

In the indirect cytotoxicity evaluation of the silk fibroin fibrous and film scaffolds, Schwann cells were seeded (at 10,000 cells/well) on bare wells of a 96-well culture plate and DMEM with 10% FBS was used to culture Schwann cells, in which the cells were allowed to attach to the wells for 24 h. Afterwards, the culture medium was replaced with the extraction DMEM (no FBS) from the scaffolds and cells that were cultured with DMEM (no FBS) were used as the control. The cells were incubated for another 24 h. The viable cells were measured by MTT assay via the UV absorbance which the high UV absorbance was also represented the high viable cells. Table 4.2. shows the UV absorbance both of indirect and direct cytotoxicity tests on the various types of substrates. To effortlessly elucidate, the data from Table 4.2. was converted to bar graphs of the viability of the cells at Fig. 4.4.

According to Fig. 4.4A, the results of indirect cytotoxicity showed that no significant difference in the viability of the cells was observed for the cells that were cultured with DMEM and the extraction media from both the fibrous and the film scaffolds, indicating that both types of scaffolds posed no threat to the cells.

In the direct cytotoxicity evaluation, Schwann cells were seeded (at 10,000 cells/well) directly onto the fibrous and the film scaffolds that were placed in wells of a 96-well culture plate. For this particular case, cells that were seeded on bare wells were used as the control. DMEM with 10% FBS was used to culture the cells and the cells were incubated for 24 h. Afterwards, the medium was replaced with serum free DMEM and then the cells were left to incubate for another 24 h. The viability of the cells was quantified by MTT assay. Fig. 4.4B shows the viability of the cells after culture on both the scaffolds and the control for 24 h. Clearly, the

the cells after culture on both the scaffolds and the control for 24 h. Clearly, the viability of the cells cultured on the bare wells (i.e., control) was greater than that cultured on both types of the scaffolds, which showed essentially similar value. This result indicated that the scaffolds, fibrous mat and film, had direct effect on Schwann cell when compared with the control.

Both tests revealed that, while both types of scaffolds did not release any substance that was detrimental to the cells, the direct contact of the cells on these materials was inferior to that of the control. Consequently, the attachment and proliferation of Schwann cells on the scaffolds at different times in culture should be further investigated to clarify the cells behavior.

Table 4.2. The UV absorbance both of indirect and direct cytotoxicity tests on the various types of substrates.

Types of substrates	UV absorbance	
	Indirect cytotoxicity test	Direct cytotoxicity test
Control	0.816	0.744
Film	0.805	0.558
Fibrous mat	0.837	0.620

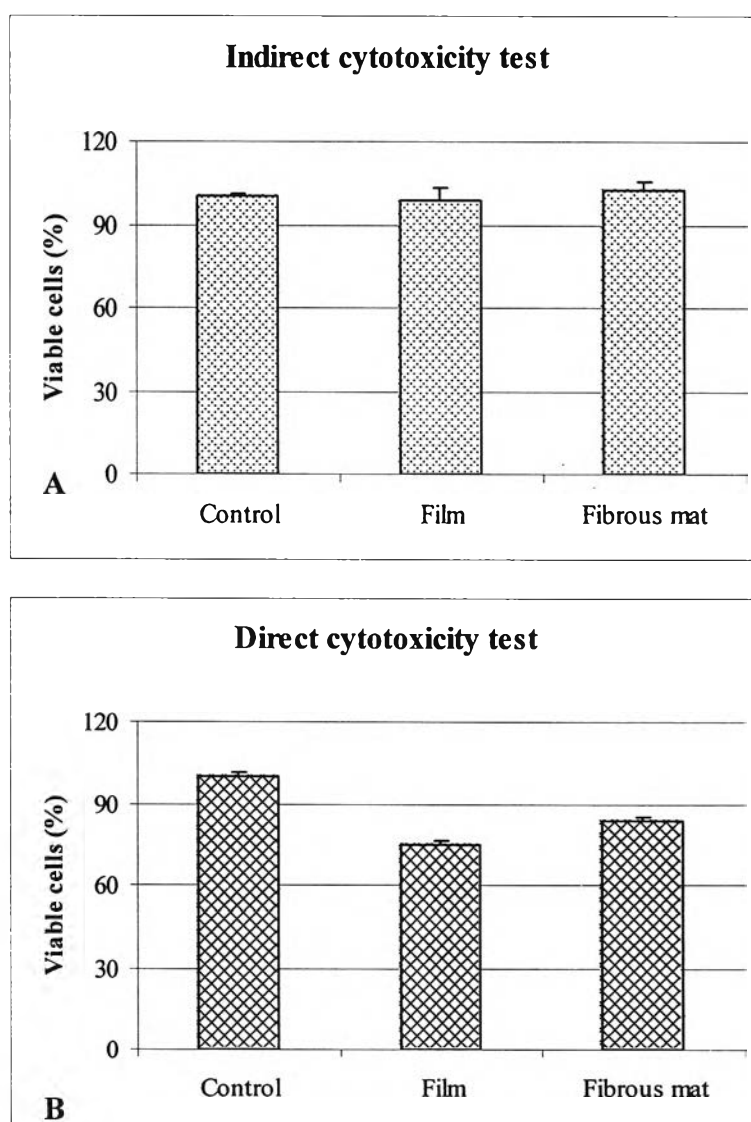


Fig. 4.4 Viability of Schwann cells (A) Indirect and (B) direct cytotoxicity evaluation of control, silk fibroin fibrous mat, and as-cast silk fibroin film scaffold.

4.5 Schwann cell attachment and proliferation

The amount of cells attached on a scaffolding material can be quantified from the MTT assay. In a previous study, Yuan et al. [25] investigated the *in vitro* interaction of Schwann cells on chitosan membranes and fibers. Their experimental results indicated that Schwann cells could grow onto chitosan materials. They reported that chitosan is a promising material for peripheral nerve repair [25].

Table 4.3. shows the UV absorbance and Fig. 4.5 shows the viability of Schwann cell attachment on silk fibroin scaffolds, both film and fibrous mat, at different culture period of 1, 2, 4, 8, and 16 h. The results were compared with the cells that were cultured on bare wells of 96-wells culture plate (i.e., control). Clearly, for any given substrate, the viability of the cells increased with increasing time in culture. During the first 4 h in culture, no significant difference in the viability of the cells was observed among various types of substrates. However, at 8 and 16 h in culture, the cells appeared to attach on the fibrous mat scaffold better than they did on the control and film, respectively.

Proliferation of Schwann cells on fibrous mat and film scaffolds at different culture period of 1, 2, and 3 days is shown in comparison with that of the cells cultured on bare wells in Table 4.4. and Fig. 4.5. It should be noted that the number of cells seeded in this case was about 5,000 cells/well (cf. the number of cells seeded in the attachment evaluation of about 10,000 cells/well). After day 1, the viability of the cells on all of the substrates was not significantly different. After day 2 and 3, the viability of the cells cultured on bare wells was significantly greater than that of the cells cultured on both types of silk fibroin scaffolds. Between day 1 and 2, it is observed that the proliferation rate of the cells cultured on control was much greater than that of the cells cultured on both types of silk fibroin scaffolds. Between day 2 and 3, continuous growth of cells on both types of silk fibroin scaffolds was apparent.

To support the above results, SEM micrographs were used to elucidate the attachment and proliferation of Schwann cells on each scaffolding material and control. Table 4.5 shows selected SEM images of Schwann cells cultured on bare wells (i.e., control) and silk fibroin fibrous mat and film scaffolds at various times.

According to these images, even after very short times in culture (e.g., 1 and 2 h), the majority of the cells seeded on the control stretched their cytoplasm along the surface, an indication of the normal phenotype of the cells. On the contrary, the cells seeded on both the silk fibroin fibrous and films were still in their round shape. After longer times in culture (e.g., greater than or equal to 4 h), the cells that were seeded on both types of scaffolds became more elongated, indicating their normal phenotype. After longer culture periods (i.e., 1 – 3 days), the cells that were cultured on both control and the silk fibroin film appeared to spread well over the surface, while those on silk fibroin fibrous mat scaffold tended to aggregate, despite the much increase in the number of cells with increasing time in culture. The result obtained suggested that Schwann cells favored the flat surface more than rough surface.

From the obtained results, these suggested that Schwann cells had a biocompatibility with the fibrous mat and film scaffold. The fibrous mat scaffold promote better of Schwann cell growth in vitro better than film scaffold did, because the fibrous mat scaffold had three-dimensional structure similar to ECM to support vascular system for oxygen or nutrient supply. However, Schwann cells favored the flat surface more than rough surface to maintain their phenotypes.

Table 4.3. The UV absorbance of Schwann cell attachment on the various types of substrates.

Times in culture (h)	UV absorbance		
	Control	Film	Fibrous mat
1	0.268	0.275	0.275
2	0.284	0.289	0.292
4	0.353	0.298	0.338
8	0.381	0.331	0.448
16	0.572	0.446	0.665

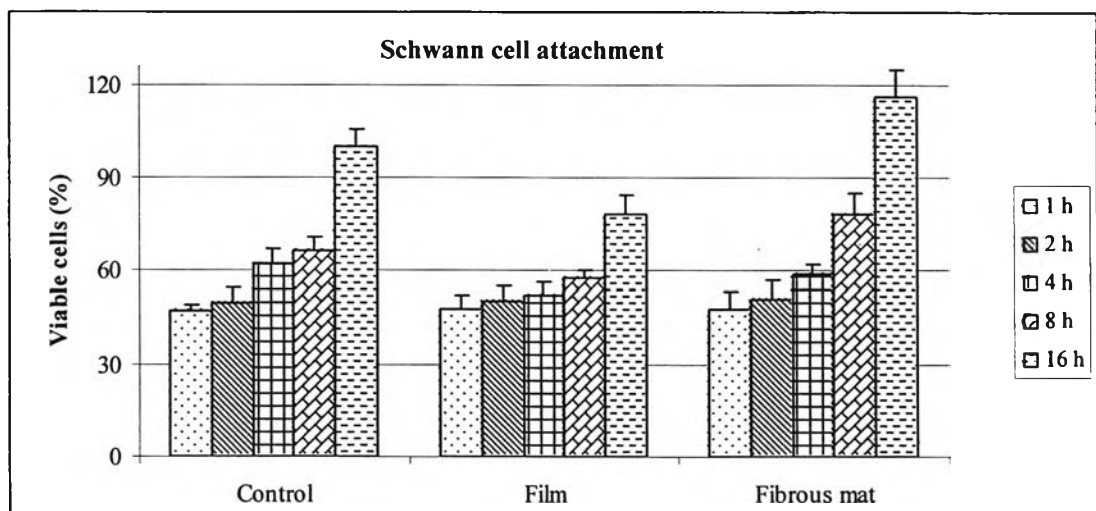


Fig 4.5. Viability of Schwann cell attachment on control, silk fibroin fibrous mat, and as-cast silk fibroin film scaffold.

Table 4.4. The UV absorbance of Schwann cell proliferation on the various types of substrates.

Times in culture [Day(s)]	UV absorbance		
	Control	Film	Fibrous mat
1	0.285	0.281	0.270
2	0.404	0.308	0.328
3	0.413	0.337	0.384

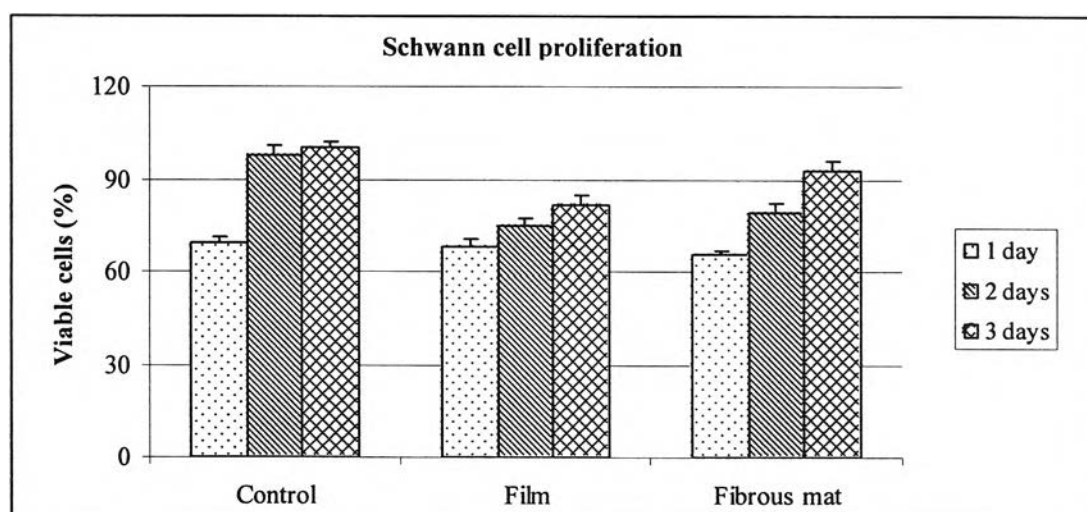
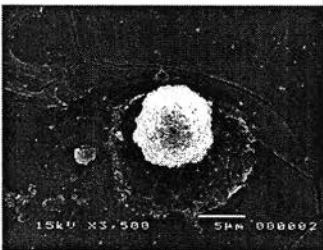
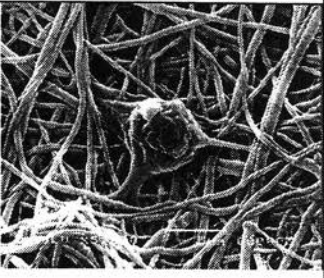
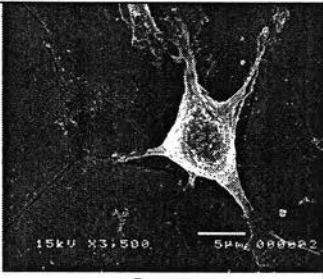
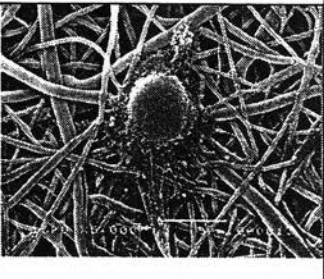
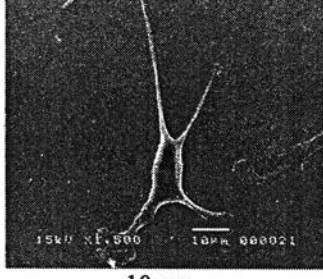
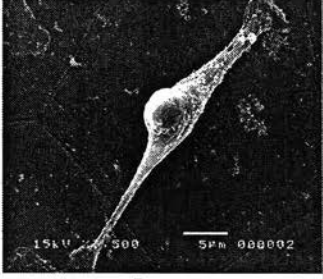
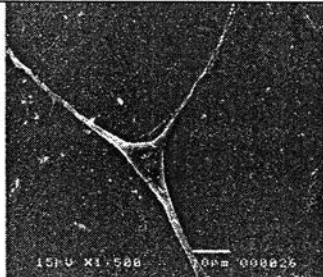
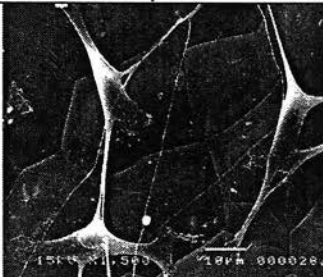
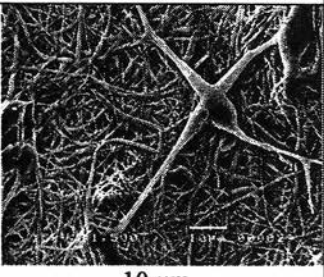


Fig 4.6. Viability of Schwann cell proliferation on control, silk fibroin fibrous mat, and as-cast silk fibroin film scaffold.

Table 4.5 The SEM images of Schwann cells cultured on the control, film, and fibrous mat at the different times in culture.

Times in culture	Materials		
	Controls	Films	Fibrous mat
1 h. Scale bar =	 10 μm	 5 μm	 5 μm
2 h. Scale bar =	 10 μm	 5 μm	 5 μm
4 h. Scale bar =	 10 μm	 5 μm	 5 μm
8 h. Scale bar =	 10 μm	 10 μm	 10 μm



